Surface-Induced Phase Behavior of Alkyltrimethylammonium Bromide Surfactants Adsorbed to Mica, Silica, and Graphite

Jun-Fu Liu and William A. Ducker*

Chemistry Department, Virginia Tech, Blacksburg, Virginia, 24061

Received: May 24, 1999

Using atomic force microscopy (AFM) to study adsorption of alkyltrimethylammonium bromide surfactants to mica, silica, and graphite from aqueous solution, we find that the sharp Krafft transition in bulk is not accompanied by a similar change in morphology at the interface. Instead, interactions between the solid substrate and the surfactant dictate an equilibrium morphology that is usually similar above and below the Krafft temperature (T_K). Mechanical properties, tested by pushing an AFM tip though the adsorbed film, do change near the T_K. In general, the film is more resistant to passage of the AFM tip below T_K, consistent with slower molecular motion. Depending on the temperature, the formation of the equilibrium structures on mica and silica proceeds by different paths. Above T_K, where micelles are present in solution, adsorption proceeds via micelle-like structures, whereas below T_K, adsorption occurs via growth of flat islands, which gradually coalesce. In some cases the adsorbed micelle intermediates were observed somewhat below T_K, probably because the negative surface potential allows cationic micelles to form in the double layer or at the interface at monomer concentrations below the critical micelle concentration. We hypothesize that the absence of a distinct structural transition near T_K at the surface of the solids is due to strong interactions that either suppress or enhance crystallization, pushing the surface transition point to lower or higher temperatures, respectively. Graphite suppresses crystallization of the bulk structure and enhances crystallization of a different structure, whereas mica and silica enhance formation of a structure that is similar to the bulk crystal. To test this hypothesis we modified the properties of one substrate, mica, through adsorption of KBr. When KBr is introduced to solution, we observed a temperature-dependent structural transition from a flat adsorbate to a cylindrical adsorbate. We propose that KBr weakens the ability of mica to template crystal formation at the interface in two ways: by adsorption of K^+ to mica in competition with alkyltrimethylammonium ions, and by interaction of Br^- with the surfactant in competition with mica anions. The cylinder/flat transition occurs over a time scale of minutes, and we are able to monitor the growth of cylinder domains on increasing the temperature and the shrinkage of these domains on decreasing the temperature.

Introduction

The phase behavior of adsorbed surfactant is of interest for technological processes such as froth flotation, wetting, and colloidal stability, all of which rely on modification of surface properties through surfactant adsorption. With the invention of atomic force microscopy (AFM)[1] it is possible to study the organization of surfactant molecules when they are adsorbed to solid−liquid interfaces,[2] and thus to compare the organization of adsorbed surfactant to the organization of surfactant in solution. In this paper, we describe a surface phase diagram for surfactants based on our AFM studies of the organization of alkyltrimethylammonium bromide surfactants on mica, silica, and graphite. There is some debate over the use of the word "phase" for an interface; we will use the expression "phase diagram" as shorthand for a map of the surfactant structure as a function of temperature and concentration.

The phase behavior of aqueous surfactant solutions is well documented.[3] Two key boundaries in the phase diagram are the critical micelle concentration (cmc), the concentration above which micelles form, and the Krafft boundary, the set of temperatures above which micelles form. (See Figure 1.) The solubility of the surfactant monomer increases with increasing temperature, so the Krafft boundary is the set of temperatures at which the solubility of the monomer reaches the cmc.

In this work, we study the effect of temperature on the organization of adsorbed alkyltrimethylammonium bromide (C_nTAB) surfactants using AFM. In particular, we focus on whether there is a surface Krafft boundary and whether it is at the same temperature as the bulk Krafft temperature, T_K. As a prelude to discussion of temperature effects, we will briefly describe the effect of the solid−liquid interface on micelle formation.

When the attraction between surfactant molecules and the solid substrate is larger than between the surfactant molecules and the solution, the surface concentration is larger than the bulk solution concentration (creating a surface excess). In other words, surface forces cause a decrease in the concentration-independent part of the chemical potential and thus a greater concentration at the surface than in bulk. Examples of such surface forces are an electrostatic attraction between the surfactant headgroup and a surface charge or a hydrophobic interaction between a hydrophobic surface group and the surfactant tail.

The surface forces that cause the surface excess of monomer may also lower the concentration-independent part of the chemical potential of the micelle and lead to micelle formation at the interface when the solution concentration is below the cmc. Charged surface groups that promote adsorption will

10.1021/jp991685w CCC: $18.00
Published on Web 09/23/1999

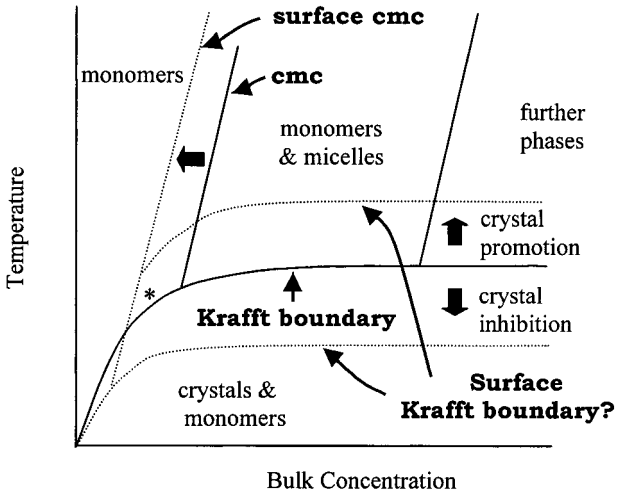

Figure 1. Schematic temperature−concentration diagram for aqueous surfactant solutions. Solid lines show boundaries for the surfactant in solution. Surface forces at the solid−liquid interface cause surface micelles to form at a lower concentration than bulk micelles. Surface forces may also influence crystal formation at the surface, leading to a shift in the Krafft boundary, either to higher temperatures (crystal promotion) or to lower temperatures (crystal inhibition). The region marked * shows where the surface micelles could form at temperatures below the bulk Krafft boundary because of a reduction in surface-critical micelle concentration.

promote micelle formation by reducing the unfavorable electrostatic interaction between headgroups. This may also cause a change in the equilibrium spacing between the headgroups and thus a change in micelle structure.[4] Strong interactions between the surfactant tail and the surface may also lead to a change in surface aggregate structure. In general, one might also expect surface micelle formation to be favored over bulk micelle formation, because adsorbed groups have already lost some conformational and translational entropy through adsorption.

Thus, factors promoting a surface excess can also promote formation of surface micelles, when the solution concentration is below the cmc, and formation of a different structure for bulk and surface micelles. AFM experiments show that sodium dodecyl sulfate (SDS) forms hemicylindrical micelles on graphite at 1/3 of the cmc,[5] hexadecyltrimethylammonium bromide (C_{16}TAB) forms aggregates on mica at 1/2 cmc,[6] and C_{16}TAB forms spherical aggregates on hydrophilic silica at 1/2 the cmc.[7] For mica and graphite, the surface structures near the cmc are different from the micellar aggregates that form at the lowest concentration in bulk.

Returning to Figure 1, we see that the knee in the monomer solubility curve means that when surface micelles form below the cmc, surface micelles could also form at lower temperatures than bulk micelles. That is, the chemical potential of molecules in the surface micelle could be less than in bulk micelles and in bulk crystals. This effect is confined to solutions just below the cmc. A more general effect could occur if surface forces affect crystallization at the surface, leading to a shift of the entire Krafft boundary at the surface. This shift is important for industrial processes that require surface micelles and are performed near the Krafft boundary. If the surface enhances the formation of crystals, surface micelles may be absent above the (bulk) Krafft boundary, and conversely, if the surface hinders crystal formation, it is possible to have surface micelles below the Krafft boundary. Presumably, the direction of the shift for the surface Krafft boundary depends on whether the surface forces exerted by a particular substrate promote an adsorbed structure that is similar to the crystal structure.

TABLE 1: Characteristics of Solid Substrates

silica	amorphous	hydrophilic, $\theta = 0°$ [a]	$-SiOH \rightleftharpoons -SiO^- + H^+$ cation exchanger
mica basal plane	crystalline	~hydrophilic, $\theta \sim 7°$	$-Si_3AlO_8K \rightleftharpoons -Si_3AlO_8^- + K^+$ cation exchanger
graphite basal plane	crystalline	hydrophobic, $\theta = 89°$	no known charging mechanism epitaxy of alkyl chains

[a] The angles refer to the contact angle of water.

Recognition of the surface Krafft boundary is somewhat problematic. Clearly we wish to measure above the cmc to avoid confusion over the effect of a surface aggregation concentration that is lower than the bulk aggregation concentration. Crystallization is accompanied by a reduction in molecular motion, so a potential method of determining surface crystallization is by fluorescence probing of microfluidity. Somasundaran and others used this technique to show that sodium dodecyl sulfate molecules have a lower fluidity on alumina than in bulk micelles.[8] In this work, we use a structural definition. We examine C_nTAB surfactants that form lamellar crystals,[9] so we use the formation of a planar surface structure in equilibrium with curved aggregates in the bulk to indicate "surface crystallization". There may be several crystal-like structures. For example, lipids form a gel phase, L_β, at higher temperatures than the crystalline phase.[10] We cannot distinguish these phases by imaging so we do not distinguish them in this work. Our definition of surface crystallization has the obvious difficulty that a flat surface layer is always counted as a surface crystal even though aggregate geometry and order are not necessarily the same. (For example, a vesicle can have almost flat walls yet still be fluid.) For flat layers, we use a large increase in the force to displace the adsorbed layer to signify the formation of a solid-like film.

The temperature is only one of several parameters that can change the chemical potential of surfactant molecules. In this paper, we have also changed the chemical potential by varying (1) the surfactant concentration, (2) the concentration of simple salt (KBr), (3) the nature of the solid substrate, and (4) the length of the alkyl chain. The following is a brief summary of how these parameters affect adsorbate structure.

Surfactant Concentration. At equilibrium, the chemical potential of surfactant is the same at the surface and in bulk, so we control the surface chemical potential through the concentration in bulk solution. The chemical potential is a weak function of concentration above the cmc, so the interesting range to study is near the cmc. As mentioned above, we find that micelles form at interfaces at about 1/2−1/3 of the cmc.

Salt Concentration. An increase in concentration of the surfactant counterion causes a decrease in electrostatic repulsion between charged headgroups, thus favoring formation of aggregates over monomers and closer packing of headgroups. This sometimes leads to formation of less curved and more closely packed aggregates.[4] Recently, we have shown that the addition of salt can also change the aggregate shape because the surfactant co-ion competes for binding sites on the solid substrate.[6]

Solid Substrate. Different solid substrates will exert different forces on the adsorbed surfactant. In this paper, we examine cationic surfactants on hydrophilic silica, mica, and graphite. Table 1 summarizes the wetting and charging properties of these substrates: silica and mica are anionic so they attract cationic molecules and micelles, whereas graphite is hydrophobic and mainly uncharged. Previous work shows that the initial organization of C_{14}TAB on silica is similar to the bulk solution structure.[11] Aggregates on mica have lower curvature than

aggregates in bulk at the same chemical potential because the crystalline mica surface ions arrange the surfactant ions with a closer spacing.[12,13] The graphite surface templates the formation of hemicylindrical aggregates[2] because of the good fit between the surfactant alkyl chains and the graphite lattice.[14] Graphite is hydrophobic, so favors adsorption of structures that maximize surface coverage in aqueous solution. This effect dominates over lattice templating for short alkyl chains.[15]

Length of Alkyl Chain. An increase in alkyl chain length increases the total attractive interaction between the surfactant tails, promoting formation of crystalline phases at lower temperatures.[10] In the absence of other interactions, increasing the tail length would be equivalent to lowering the temperature. If the surfactant alkyl chain has significant interactions with the interface (e.g., graphite), then a longer alkyl chain should also enhance any effect due to surface bonding. Later we show that, for our system, temperature changes are not equivalent to changes in the length of the alkyl chain.

Materials and Methods

Samples and Substrates. The solid substrates were muscovite mica, fused silica, and graphite. Muscovite mica (S&J Trading, N. Y.) or graphite from a pyrolytic graphite monochromator (grade ZYH, Advanced Ceramics Co.) was freshly cleaved immediately before each experiment. We always monitored surfactant adsorption within regions that were free of steps so that we observed adsorption to the "atomically smooth" basal plane. The spacing between steps was about 500 nm on graphite; we never found steps on the mica surface. Polished silica substrates (Heraeus Amersil Inc., GA) were cleaned by heating in hot concentrated sulfuric acid (95.7%, analytical grade, Baker, USA) for more than 12 h then thoroughly washing with water. Silica substrates were accepted for adsorption measurements if a uniform thin film of water formed on the surface when they were exposed to steam (the "steam test").[16] Silica surfaces passing this test were completely wet by water. The surface of the silica substrates had undulations that were about 0.5−1 nm high separated by about 150 nm. Over a scale of 50 × 50 nm the measured rms roughness was 0.016 nm, but this is probably just noise and does not account for the inability of the tip to resolve highly curved features. Water was prepared by an Easypure UV system (model D7401, Barnstead Thermolyne Co., Dubuque, IA). The water had a conductivity of 18.3 MΩ/cm at 25 °C and a surface tension of 71.5 mJ/m^2 at 25 °C. Hexadecyltrimethylammonium bromide (C_{16}TAB, 99%, BDH, Poole, U.K.) and octadecyltrimethylammonium bromide (C_{18}TAB, Aldrich, Milwaukee, WI) were each recrystallized three times from a distilled acetone/water mixture. Eiconsanyltrimethylammonium bromide (C_{20}TAB, synthesized by Tim Davey, University of Otago) was recrystallized three times from an ethyl acetate/ethanol mixture. Dodecyltrimethylammonium bromide (C_{12}TAB, 99%, Aldrich, Milwaukee, WI), and potassium bromide (>99%, Aldrich, Milwaukee, WI) were used as received.

Atomic Force Microscopy. Images were captured in situ at the solid−liquid interface using a Nanoscope III AFM (Digital Instruments, CA) using silicon cantilevers (Park Scientific, CA) with nominal spring constants of 0.06 N/m on silica substrates, and silicon nitride cantilevers (Digital Instruments, CA) with nominal spring constants of 0.32 N/m on mica and graphite substrates. Spring constants were not calibrated independently because the force depends on the radius of the tip, and this was also not known. For any one figure in this paper, we have used a single cantilever, so that results within a figure are all scaled by the same factor. Prior to use, the cantilevers were irradiated in a laminar flow cabinet with ultraviolet light (~9 mW/cm^2 at 253.7 nm) generated from a Pen-ray lamp (UVP, Inc., Upland, CA). The irradiation time was about 40 min for the first use and 10 min for subsequent use. The solution was held in a fluid cell and sealed by a silicone O-ring. For each experiment, the fluid cell and the O-ring were cleaned first with water and then distilled ethanol (Aaper Alcohol Chemical Co., USA).

Images record cantilever deflection while integral and proportional gains were in the range 0.5−1, and scan rates were in the range 5−10 Hz. Distances in lateral dimensions were calibrated by imaging a diffraction grating replica of a 2160 lines/mm waffle pattern in the range 20−60 °C. The voltage-distance coefficient of the piezocrystal was constant over this range. Distances normal to the surface were calibrated by measuring the depth of the bars of the grid pattern (31 nm deep).

Images were captured when the AFM tip was as close as possible to the surfactant film while maintaining a stable image, i.e., on the high gradient portion of the repulsive force curve before the instability. This is consistent with the conditions of close proximity and a high gradient in signal that usually give high resolution in near field microscopy. Although imaging of adsorbed surfactants is sometimes referred to as double-layer imaging,[2] double-layer forces tend to have smaller gradients than short-range hydration/protrusion/overlap forces, so double-layer forces may actually lower the resolution of surfactant aggregates by increasing the area on the tip and sample over which data is collected. Soft-contact imaging[17] may be a better name. To avoid the low gradient double-layer forces, we image at high force where the gradient is higher. However, imaging at high force is undesirable from a practical point of view because the tip is near a mechanical instability, and it is undesirable from a scientific perspective because the film is most perturbed from the isolated case. That double-layer forces are unnecessary is clearly seen from the ease with which uncharged surfactants can be imaged.[12,15,17,18] In the absence of double-layer forces, uncharged surfactants can be imaged at a high force gradient, but at a low force.

Control and Measurement of Cell Temperature. The cell temperature was varied using a Peltier device under the solid sample. Please note that since the solution was heated from below only, there was a small temperature gradient of about 1 °C/mm normal to the solid−liquid interface. This introduced errors in our temperature measurement, and means that after a long time, our systems are in a steady state, which approximates equilibrium. The temperature was measured using a small thermistor, placed between the sample and the Peltier device. Ideally we would like to measure the temperature inside the fluid, but we were unable to fit a thermistor inside the cell when the tip was in contact with the sample. Instead, we calibrated the temperature inside the cell (while not imaging) relative to the temperature under the cell. This calibration depends on the gradient of temperature across the sample, so the calibration was done separately for each of mica, graphite, and silica. The temperature was measured using a thermistor (model 8402-10, Cole-Palmer Instrument Company, Vernon Hills, IL) which was calibrated against a NIST-traceable thermometer. We also calibrated the cell temperature by measuring the melting point of zinc nitrate hydrate (99.999%, mp 36 °C, Aldrich, Milwaukee, WI) for each substrate. Discrepancies in calibration suggested that our systematic error in temperature was about ±1 °C for silica and ±0.6 °C for mica.

Preparation of Solutions. Solutions that were examined above room temperature were heated before injection into the

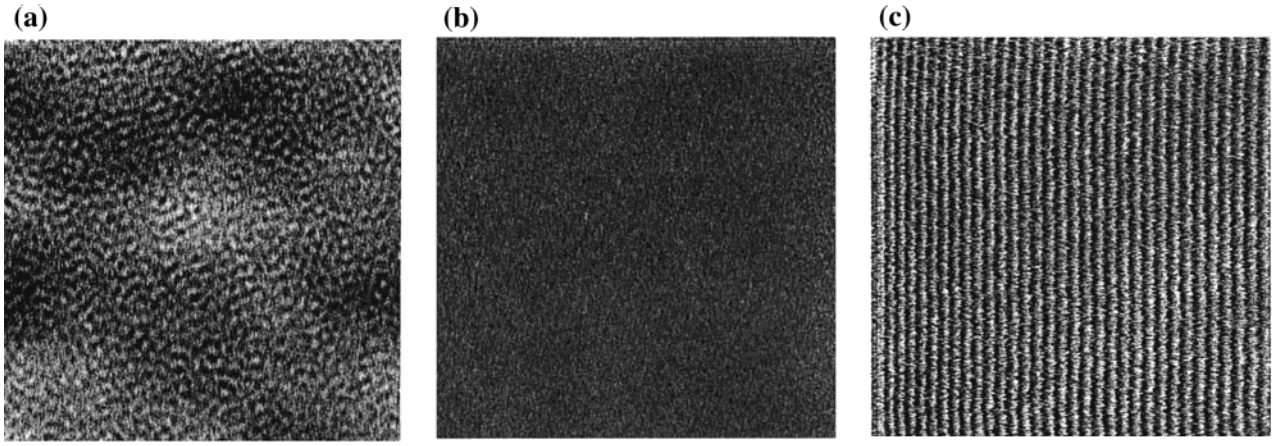

Figure 2. AFM images of types of adsorbed surfactant structures (300 nm × 300 nm). (a) C_{16}TAB on silica at 25 °C and 2 cmc (spheres or hemispheres on a monolayer). (b) C_{18}TAB on mica at 25 °C and 2 cmc (flat). (c) C_{18}TAB on graphite at 26 °C and 2 cmc (hemicylinders).

TABLE 2: Summary of Equilibrium Structures above T_K

	equilibrium structure above T_K	comparison to bulk structure
silica	C_{14},[a] C_{16}: ~spherical	relatively unperturbed
	C_{18}, C_{20}: flat	flattened
mica	C_{12}, C_{14}[a]: cylindrical	all structures highly perturbed from solution
	C_{16}, C_{18}, C_{20}: flat	due to closely spaced counterions on substrate
graphite	C_{14},[a] C_{16}, C_{18}, C_{20}: hemicylinders	highly perturbed from solution because of alkyl−substrate epitaxy

[a] Data from ref 11.

AFM fluid cell. The preequilibration temperature was not always identical to the fluid cell temperature, but care was taken to ensure that the Krafft boundary was not crossed on injection into the cell. This was particularly important for C_{18}TAB and C_{20}TAB, which have Krafft temperatures well above room temperature. For measurements below the Krafft boundary, a concentration above the solubility limit means that we injected the supernatant above a saturated solution. We also cooled solutions through the Krafft boundary in the fluid cell. Crystal formation usually prevented AFM measurement, but on occasions when it did not, we recorded the same structures as when the saturated supernatant was injected.

Results and Discussion

Surface Geometry above the Krafft Temperature. The measured surface structures above the Krafft temperature are summarized in Table 2, and Figure 2 shows AFM images of the various structures. In every case, the symmetry of the aggregate was not a function of temperature above T_K. Adsorption is an exchange process, involving removal of some water and counterions from both the solid and the surfactant and bonding between the solid and the surfactant. We interpret changes in structure in terms of changes in this bonding.

Silica. AFM images of C_{16}TAB on silica (Figure 2) are consistent with adsorbed micelles and look similar to those recorded previously by Manne et al. for C_{14}TAB on silica.[11] Neutron reflectivity studies show that C_{16}TAB forms two layers on the silica, and that on rough silica, the two layers are different.[19] The AFM image does not record the structure beneath the outer layer of surfactant, so the image could also result from hemispheres on top of a flat C_{16}TAB monolayer. (See Figure 3.) The force between a silicon tip and the sample shows a jump-in of about 4.4 nm (Figure 4), which is about twice the extended length of one C_{16}TAB molecule. If the adsorbed layer is similar on the tip and the silica sample, then after the jump-in, the tip is resting on the inner layer of surfactant on both tip and sample. Imaging at this tip−sample separation at a variety of forces does not reveal any features and is consistent with a flat inner layer. This does not necessarily mean that the inner layer is flat when the surfactant film is isolated because the surfactant-coated tip exerts different forces to an unperturbed film. When the tip is pulled off this layer, there is significant adhesion. There is no adhesion when the tip is pulled off bare silica, reinforcing the concept that there is still surfactant under the tip. After the AFM cell is rinsed thoroughly with water, no micelle-like structures are observed. The adhesion is large, suggesting that a hydrophobic film now covers the silica. In summary, the outer layer of the adsorbed structure is curved and discontinuous, but the inner layer is either flat, or is readily converted from micellar to flat by removing the outer layer either with an AFM tip or by rinsing with water.

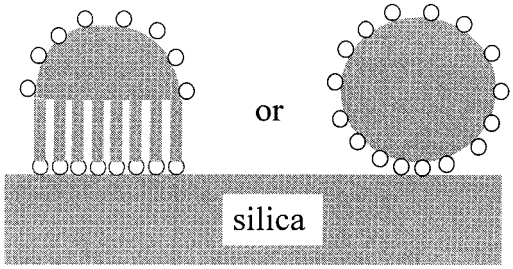

Figure 3. Schematic of C_nTAB micelles on silica. The image is consistent with either a half-micelle on a flat monolayer or a full micelle.

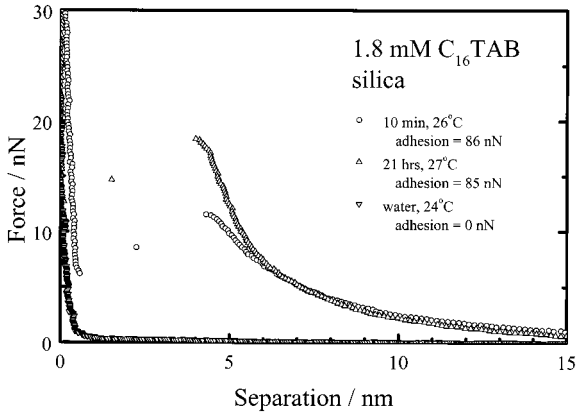

Figure 4. Force between silicon tip and silica sample in water or 2 cmc C_{16}TAB solution above the Krafft temperature.

TABLE 3: Characteristics of Surfactant Aggregates Adsorbed to Silica−Solution Interface[a]

surfactant	C_{12}TAB	C_{16}TAB	C_{18}TAB	C_{20}TAB
cmc /mmolL^{-1}	15	0.9	0.29	0.05
concn /cmc	2	2	0.9	2
2 × molec length /nm	3.56	4.54	5.02	5.52
Krafft temp (T_K) /°C	<0	25	36	46
equilibrium morphology above T_K	spheres	spheres	flat	flat
max temp studied	56	65	56	56
initial morphology above T_K	spheres	spheres	spheres	spheres
(T_K surface − T_K bulk) /°C for metastable micelles		< −7	−5	0
sphere period /nm	6.4	9.4	14	14
thickness[b] /nm	3.6	4.6	5.1	5.1
thickness[c]/nm	3.8	4.7	5.5	5.3
equilibrium morphology below T_K		spheres	flat	flat

[a] Thickness values are the distances that the AFM tip jumps from a repulsive force to the solid substrate, so are subject to errors due to (1) compression of the film by the tip and (2) instability caused by attractive forces. In all cases, the thickness is about twice the length of the all-trans molecule, consistent with a micellar structure. The Krafft temperatures were measured at the solution concentration specified. [b] Measured while tip is scanned normal to substrate. [c] Measured while tip is scanned parallel to substrate.

C_{18}TAB and C_{20}TAB both initially adsorb to silica in the form of micelles (Table 3 and *Kinetics of Adsorption*) but the equilibrium structures are flat layers. After penetration of the outer layer with the tip, or washing with water, the structure is also flat.

Mica. C_{12}TAB[20] and C_{14}TAB[11] adsorb as cylindrical structures whereas the C_{16}TAB, C_{18}TAB, and C_{20}TAB form flat layers. C_{16}TAB initially forms cylindrical aggregates, but these transform to a flat sheet over about 17 h.[6]

Comparison of Bulk and Surface Structures. $C_{12,14,16}$TAB all form approximately spherical micelles in solution near the cmc,[21] and C_{18}TAB forms spherical micelles coexisting with a few disklike micelles.[22] The AFM results on silica and mica exhibit two trends: the surfactants often form less-curved aggregates on solid substrates than in solution, and longer alkyl chains tend to form more eccentric (or even flat) structures on silica and mica. Both of these effects have been discussed earlier for mica.[12,13,23] Possible explanations for the flatter aggregates at the interface compared to bulk solution (at the same chemical potential) are:

(i) Smaller repulsion between charged headgroups because of the close proximity of bound anionic groups on the solid. This argument relies on the inner surfactant layer exerting a strong influence over the outer surfactant layer (that we observe by AFM).

(ii) The spacing between micelles on the surface is much smaller than in bulk solution, leading to much larger repulsive forces between the micelles. In bulk solution at high mole fraction these forces favor structures such as cylinders and flat sheets which have fewer intermicelle interactions.[24] The same mechanism may operate at the interface.

(iii) The solid substrate is planar, providing a planar template for the surfactant aggregate. This effect should be greater for mica, which is smooth compared to the radius of the micelles.

(iv) Through adsorption, the surfactants have already lost some entropy, decreasing the penalty for forming larger aggregates. The entropy penalty is a driving force for forming small micelles in bulk.[4]

Possible reasons for the formation of bilayer structures for the longer alkyl chains are:[25]

(a) An increase in packing parameter[24] because the volume increases linearly with the surfactant tail length, but the effective length of the surfactant tail may scale with a fractional power.[17]

(b) Shorter chain surfactants have higher cmcs and thus the solution has a greater activity of bromide counterions at the cmc. These counterions compete with surface anions for charged headgroups, reducing the effect of factors (1) to (3) above.

Neutron scattering measurements show that $C_{12,14,16}$TAB micelles *in bulk* all have about the same eccentricity (1.1) in 50 mM solutions.[21] This appears to be inconsistent with point (a) above. The same neutron scattering studies show that a change in type or concentration of anion has a significant effect on eccentricity. For example, the eccentricity is 1.4 in 50 mM $C_{16}TANO_3$ and 1.9 in 200 mM C_{16}TAB. Adsorption to an anionic solid causes substitution of bound surface counterions in place of solution counterions so the surfactant aggregate shape can change because the solution and surface anions have different affinity for the surfactant ion as well as different densities.

Comparison of Structures on Mica and Silica. A flat sheet is observed for a shorter chain on mica than on silica (C_{16} vs C_{18}), and the curved aggregates are cylinders on mica and spheres on silica. Examining our list of four possible explanations, it is tempting to suppose that the anionic sites on mica are either more closely spaced or have a higher affinity for quaternary ammonium headgroups than the sites on silica. In support of this idea, we have shown that the addition of extra salt to C_{16}-TAB causes more curved aggregates on mica, apparently by using up some of the anionic sites.[6] Thus the mica can be made silica-like. However, we have not been able to make the silica mica-like. We attempted to do this by adding 10^{-3} mol/L KOH to replace SiOH groups with SiO^-K^+, but the aggregates remained as spheres under this condition. The same result was observed for C_{14}TAB on silica.[11] Thus, the silica was not made mica-like merely by increasing the density of available binding sites.

A possible explanation for the difference between structures on mica and silica is the difference in surface roughness. The mica surface is crystalline and smooth whereas the silica is amorphous. Aggregates that have a large contact area with the surface (bilayers and cylinders) will either incur a bending energy to attach to a curved surface or a dissociation energy to partially detach from the surface. In contrast, a spherical micelle attaches over a small area and may not be influenced by longer scale curvature of the substrate. Thus we might expect a surfactant that forms cylinders on a flat substrate to form spheres on a rough surface. Fragento et al.[19] found an increase in water content for adsorbed surfactant films on silica when the silica was made more rough, which is consistent with a change to discontinuous aggregates.

A final point to consider is competition of solvent water for surface sites. Our silica is very hydrophilic (it passes the steam test), so one would expect water to occupy more surface sites on silica than on mica, favoring curved aggregates. To test the effect of wettability, we adsorbed C_{16}TAB to silica that had a finite contact angle (5∼10°). Spherical micelles formed on this substrate, so a small change in wettability did not exert a large change in micelle shape.

Transitions well above the Krafft Temperature. We expected that the continuous structures observed on mica and silica might break up into discontinuous structures at temperatures well above the Krafft temperature. On mica the structure was continuous 15, 27, 17 °C above T_K for C_{16}, C_{18}, and C_{20}, respectively, and on silica the structure was continuous up to

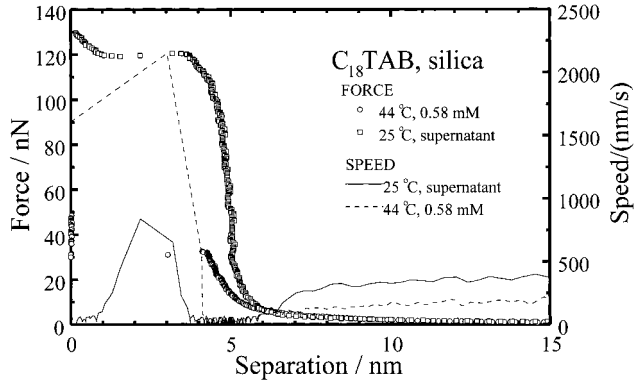

Figure 5. Force between silicon tip and silica sample in 2 cmc C_{18}TAB above or below T_K. The same tip was used for both measurements. The force barrier is much higher below T_K, and the force increases when the film thins. A three-point average of the speed that the tip approaches the silica is also shown. The tip moves more slowly through the film below T_K than above T_K. The approach speed in the absence of force was 300 nms^{-1} below T_K and 600 nms^{-1} above T_K.

20 °C and 10 °C above T_K for C_{18} and C_{20}, respectively. Thus, we did not observe transitions far from T_K.

Graphite. Hemicylinders were observed on graphite for C_{12}, C_{16}, C_{18}, and C_{20}TAB. Earlier Manne et al. also observed hemicylinders for C_{16}TAB.[2] The hemicylindrical structure of surfactant on graphite has been attributed to ordered packing of the first layer of alkyl chains parallel to the graphite−solution interface,[2] which in turn has been attributed to the match in size of two surfactant methylene units to the unit cell of the exposed graphite surface.[14] Presumably the good match in size allows the alkane to lie very close to the graphite lattice and form strong van der Waals forces. The ordered packing of the first layer of surfactant templates the formation of a hemicylindrical aggregate.[2] The electrostatic attraction between the positive surfactant headgroups and the mobile electrons in the conducting graphite surface may also help to stabilize the closely spaced headgroups.

Structures below the Krafft Boundary. *Silica.* Table 3 summarizes our results on silica. The low-temperature structure for C_{18}TAB and C_{20}TAB was a featureless layer. Adsorption of this featureless layer was distinguished from no adsorption by the difference in force curve. (Compare Figure 5 to Figure 4 (water).) The force curve is similar in general shape to that measured on a bilayer above T_K: the force is repulsive and exponential, consistent with hydrophilic headgroups facing solution and a double layer of counterions. The nature of the adsorbed film was also probed by pressing an air bubble against a sheet of mica that had been exposed to C_{18}TAB for 24 h. The bubble could not be made to attach to the mica, indicating a hydrophilic surface and thus orientation of headgroups into solution. The force curve below T_K shows that surfactants can still be used to modify wetting and colloidal stability below the Krafft temperature. Association of molecules at the surface proceeds against an electrical potential even when there are no micelles in solution.

The salient differences below the Krafft temperature were that (a) there was no metastable micellar adsorbate and (b) the force barrier was usually much greater.

The force required for the tip to penetrate the low-temperature layer was much greater than the force required to penetrate a layer of surface micelles. Possible reasons for this are (1) the low-temperature layer is more crystalline or (2) it is easier for a tip to push micelles to the side than to penetrate a continuous film. We were prevented from making an unambiguous comparison between the equilibrium barrier height above and below T_K because we could not maintain high temperatures for a long time in the AFM without evaporation.

TABLE 4: Structures on Mica in C_nTAB-Only Solution

n	12	16		18				20	
$T - T_K$/°C	>25	−6	4	−10	14	−10	14	−20	13
concn /cmc	2	2	2	0.9	0.9	2	2	2	2
structure	cylinders	flat	flat	*a*	flat	flat	flat	flat	flat
thickness	2.7	2.4	4.3		3.4	3.4	3.8	2.7	3.7

[a] No adsorption within 1 day.

The AFM tip also moves more slowly through the surface film below T_K. Above T_K, there is a threshold force beyond which the film yields and the tip rushes through, whereas below T_K the tip passes through the film slow enough that we can measure the force in the film. (See Figure 5.) This suggests slower molecular motion in the low-temperature film.

For C_{16}TAB on silica, we observed approximately spherical micelles at $T_K - 5$ °C (20 °C) even after 16 h of equilibration. Thus, silica does not appear to promote the formation of a flat layer for C_{16}TAB. This is in contrast to the behavior of C_{18}TAB and C_{20}TAB. The lower limit of our temperature control is $T_K - 7$ °C (18 °C). At $T_K - 7$ °C, AFM images show vague lumps that loosely resemble the micelles imaged at higher temperatures. The gradual loss of distinct micellar structures from about 24−18 °C leads us to suspect that a flat layer might exist at lower temperatures.

Mica. Below T_K, saturated solutions of $C_{16,\ 18,\ 20}$TAB all form flat layers on mica. Above T_K at 2 cmc, flat layers were also formed. Force measurements are consistent with an interaction between two films with headgroups facing solution. Thus, the substrate forces a "crystal-like" structure at all temperatures. When we apply a force to the adsorbed film with the AFM tip, there is always a threshold force at which the layer yields. The distance that the tip moves gives an estimate of the thickness of the adsorbed surfactant layer. (See Table 4.) The jump-in is less than twice the extended length of the molecule for C_{16}TAB below T_K, and for C_{18}TAB or C_{20}TAB above or below T_K, consistent with some interdigitation of surfactant tails as in crystals of C_{16}TAB. Equilibrium structures were achieved slowly on mica; the kinetics are discussed in a later section.

Mica in Salt Solutions. We used salt to modify the organization of alkyltrimethylammonium bromides above the Krafft boundary. Our thinking is that the addition of salt is a mechanism for changing the mica substrate. Previously we have shown that the addition of alkali−halide salts above the Krafft boundary leads to a transition from a flat layer to cylinders for C_{16}TAB or spheres for C_{16}TACl.[6] This was attributed to competition between the surfactant cation and the metal ion for surface sites. Presumably, Br^- also weakens the effect of mica by competing with mica anions for surfactant headgroups. We found similar behavior for C_{18}TAB and C_{20}TAB: addition of KBr led to a transition from a flat structure to a cylindrical structure. Further increases in KBr concentration caused the cylinder axis to wander and the cylinders to become shorter. The concentration of KBr required to break up the flat layer structure was a function of temperature and the length of the alkyl chain. For a given salt concentration, we observed a transition from a flat structure to cylinders as the temperature was raised. As salt was added, the transition from flat to cylindrical surface structures occurred at a lower temperature. (See Table 5.) Figure 6 is a schematic representation of how

TABLE 5: Temperature of the Transition between Flat and Cylindrical Structures on Mica[a]

surfactant	[KBr] /mM	trans temp /°C	bulk T_K /°C	$T_{min} - T_K$ /°C	$T_{max} - T_K$ /°C
C_{16}TAB	10	<23	27	−2	+17
C_{18}TAB	0	(63)	36	−14	+27
C_{18}TAB	10	44	39	−10	+14
C_{18}TAB	100	35	41	−18	+9
C_{20}TAB	0	(63)	46	−19	+17
C_{20}TAB	10	(55)	49	−23	+6
C_{20}TAB	100	46	50	−27	+6

[a] For each surfactant, the concentration was held constant at twice the cmc in the absence of salt. Values in brackets indicate the maximum temperature studied: the observed structure was always flat. If there is a transition, it is at a higher temperature. Our measured values of the bulk T_K are shown for comparison. The last two columns show the minimum (T_{min}) and maximum (T_{max}) temperatures that we studied.

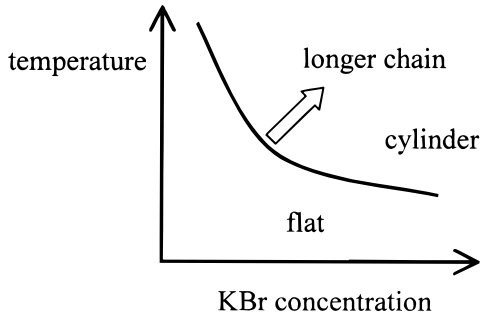

Figure 6. Rough outline of phase diagram for C_nTAB on mica. At the mica−water interface, cylindrical micelles are promoted by a higher temperature, a shorter alkyl chain, or a higher solution concentration of KBr. KBr has opposite effects in solution and at the interface: it raises T_K in solution but promotes formation of cylindrical micelles rather than flat sheets on the mica surface.

we believe that temperature, KBr concentration, and chain length interact to give the boundary between flat and cylindrical surface aggregates.

Table 5 also shows our measured values of T_K. We find that the addition of salt raises T_K (favors the formation of crystals over micelles in bulk). This is in contrast to the concomitant reduction in temperature of the flat-cylinder transformation at the surface and indicates that the effect of salt on adsorbed structure is related to the mica surface. At the mica surface, there are negative lattice sites that can bind cations—either CTA^+ or K^+ ions. In the absence of K^+, the quaternary ammonium ions are probably packed closely in a planar array matching the lattice ions. This promotes the formation of a crystal-like structure. When K^+ is added, some of the anionic sites are used up by the K^+ so this templating is weakened, and the surfactant forms a structure more similar to the solution micelle. Br^- may also enhance cylinder formation by screening attractive mica−C_nTAB interactions that cause flat aggregates and repulsive micelle−micelle interactions that discourage discrete aggregates. Thus, with increasing salt concentration, the mica becomes less crystal promoting. The effect of salt is so strong that, despite the fact that mica suppresses micelle formation, C_{18}TAB forms micelles at the interface between mica and 100 mM KBr solution, even when micelles do not occur in bulk solution.

Graphite. The structure on graphite was always hemicylindrical. We investigated a wide range of temperatures, from 30 °C above the Krafft temperature to 11 °C below the Krafft boundary for C_{18}TAB. The structure was also hemicylindrical for all $C_{12,16,18,20}$TAB at room temperature. These represent conditions from at least 24 °C above to 21 °C below the respective Krafft boundaries. We expected to see some transformations: perhaps formation of a flat layer at a very low temperature, as a result of crystallization, or perhaps formation of a flat layer at high temperature as entropy overcame the bonding between the graphite and the alkyl chain. The lack of transformation shows the strength of the interaction between the alkyl chain and the graphite. Why does the graphite so strongly inhibit formation of crystals with the bulk structure? The AFM images of adsorbed C_nTAB are consistent with tail-to-tail packing. STM images of alcohols also show tail-to-tail packing of alcohols on graphite.[14] (For STM, the resolution is sufficient to determine the positions of the oxygen atoms.) In a crystal of C_{16}TAB the molecules stack in sheets which are slightly more than one molecule thick (2.6 nm compared to the molecular length of 2.2 nm).[9] Nearest neighbors within the sheet are antiparallel (interdigitated) and nearest neighbors between sheets have parallel orientation. Thus, the first layer of molecules on the graphite does not represent a cut through any orientation of the crystal. Thus the adsorbed layer has a large period mismatch or an orientational mismatch so the graphite templates the formation of an alternate structure and inhibits the formation of the bulk crystalline structure. These ordered hemicylinders on graphite may be useful for templating other nanostructures.

TABLE 6: Repeat Period for Hemicylindrical Micelles on Graphite[a]

surfactant	C_{12}TAB	C_{16}TAB	C_{18}TAB	C_{20}TAB
concn /mM	30	1.8	0.26	0.10
T /°C	23	24	26	23
period /nm	7.1	9.1	9.3	9.7
2 × molec length /nm	3.56	4.54	5.02	5.52
κ^{-1} /nm	2.4	10	18	43

[a] κ^{-1} is an estimate of the Debye length assuming that only monomers and their counterions are present.

TABLE 7: Summary of Substrate Effects on Surfactant Crystallization

silica	enhancement of crystal-like structure for C_{18}TAB, C_{20}TAB suppression of crystal-like structure for C_{16}TAB
mica	enhancement of crystal-like structure adsorption of salt reduces enhancement of crystallization
graphite	strongly promotes ordered structure different from crystal

We have also measured the length of the repeat unit normal to the cylinder axis as a function of chain length. (See Table 6.) This repeat unit is the sum of the hemicylinder diameter and the separation between hemicylinders. Between C_{16}TAB and C_{20}TAB, the period increases by slightly less than the increase in extended length of two molecules (0.6 nm vs 1.0 nm). Between C_{12}TAB and C_{16}TAB, the period increases by much more than the increase in extended length of two molecules (2.0 nm vs 1.0 nm). For C_{12}TAB, the solution Debye length is smaller than the separation between hemicylinders, so repulsive forces are well screened. The greater screening for C_{12}TAB is consistent with closer approach of two hemicylinders on the graphite surface.

Summary of Surface Effects near T_K. Table 7 summarizes the effects of the silica, mica, and graphite on the crystallization of C_nTAB. Mica promotes formation of crystal-like structures well above the bulk Krafft temperature, graphite promotes an alternate structure at all concentrations, and the behavior of silica depends on the surfactant.

Kinetics of Adsorption. *Silica, Adsorption below T_K:* C_{18}TAB is slow to form equilibrium structures on silica at room temperature ($< T_K$) and the adsorption is featureless. Figure 7 shows the force between a silicon tip and silica as a function of time since exposure to the C_{18}TAB solution. In water the force is repulsive because of double-layer and hydration forces. In

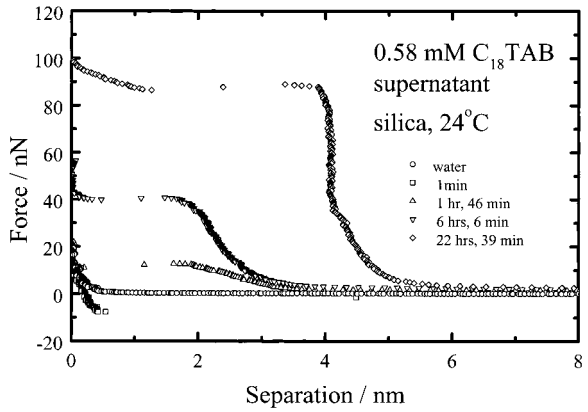

Figure 7. Force between silicon tip and silica sample in 2 cmc C_{18}-TAB below T_K as a function of time.

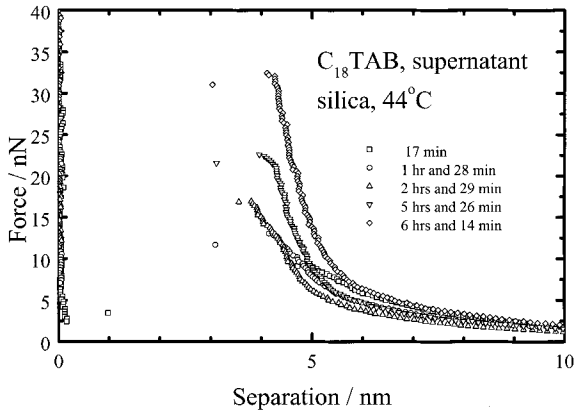

Figure 8. Force between silicon tip and silica sample in 2 cmc C_{18}-TAB above T_K as a function of time.

the early stages of adsorption there is a slight attractive force, possibly the result of van der Waals forces as adsorption makes the surface less charged and less hydrophilic. With time, the force becomes repulsive and an instability is observed. We interpret the repulsive force as the hydration/protrusion/double-layer forces due to the headgroups of the surfactant facing solution and the instability as the force required for the tip to penetrate the adsorbed layer. The magnitude of the force barrier before instability increases with time up to about 22 h of adsorption, which suggests that the alkyl chains become more densely packed with time. Up to about 6 h the thickness is about 2 nm or one molecular length, suggesting that the surfactant molecules are interdigitated. By 22 h, the film has become twice as thick, suggesting that either there are two interdigitated films or that two layers of opposite orientation have formed (i.e., a conventional bilayer). The height of the barrier also increased with time for C_{20}TAB. Below T_K, there is very slow formation of a crystal-like structure.

Samples that were first equilibrated (e.g., 24 h) then rinsed with water showed strong adhesion in the force curve, and the classical repulsive instability for surfactant layers was no longer present. An air bubble readily attached to this surface, with a low air contact angle. This suggests that the molecules in the bilayer with headgroups facing the solution are readily desorbed, but the molecules in the bilayer with headgroups facing the silica remain to leave a hydrophobic surface. When surfactant solution was injected into the cell again, the instability appeared immediately and the height of the barrier was about the same as before rinsing with water. So, the adsorption of the second layer in the presence of the first layer is very fast, even in the absence of micelles.

Silica, Adsorption above T_K. Although the equilibrium structures for $C_{18,\ 20}$TAB are flat above and below T_K, formation of the films follows quite different routes. Initial adsorption above T_K is rapid (minutes) and the adsorbate forms approximately spherical micelles. It may be that micelles from solution are the adsorbing species: micelles are more highly charged than monomers, so will experience a stronger attractive force when they approach a vacant region of silica.

The surface micelles are stable for several hours, so are quite amenable to investigation. These *metastable* micelles are very similar to the stable micelles observed in C_{16}TAB solution. If the silica is rinsed with water then there is a large adhesion. This is consistent with the remaining layer consisting of surfactant with tails facing solution. If C_{18} TAB or C_{20}TAB is reintroduced, then the micelles adsorb within minutes. Our proposed structures are thus the same as those in Figure 3. We studied these metastable micelles as a function of temperature and found that the threshold temperature for surface micelle formation was T_K for C_{20}TAB. This is reasonable, as there are no micelles in bulk solution below this temperature. For C_{16}-TAB and C_{18}TAB, the initial structure is surface micelles even below T_K. Apparently silica either promotes the formation of micelles in the double layer,[26] which then adsorb, or promotes the formation of surface micelles from adsorbed monomers. For C_{18}TAB and C_{20}TAB these micelles then transform into a flat layer. The results are summarized in Table 3.

The force curve on the micelles is similar to that observed on the bilayer at low temperatures, but the barrier height is initially much smaller. (See Figure 8.) Over a period of hours, the height of the barrier increases and the layer transforms to a flat sheet. The decrease in ease of passage of the AFM tip to the silica surface reflects an increase in organization of the surfactant tails or the loss of the ability of the molecules to move sideways as the film goes from discontinuous to continuous.

We were interested to know whether the slow transformation from spheres to flat was due to an effect at the solid side (inner layer) or the liquid side (outer layer) of the surfactant film. Chen et al. have described a model for C_{16}TAB adsorption to mica in which trapped M^+Br^- ions slowly leave the surfactant film, thus allowing an increase in binding of $C_{16}TA^+$ in the inner layer to mica.[27] To examine for similar effect on silica, we left silica exposed to C_{18}TAB solution until the initially adsorbed spherical micelles converted to a flat layer, and then flushed with water. A featureless layer was still observed, but the force changed from repulsive (Figure 8) to attractive, with no mechanical instability. We interpret this as the removal of the outer layer of surfactant and exposure of the hydrocarbon tails of the inner layer. When we reintroduced C_{18}TAB solution to the cell, we immediately observed a flat layer and a large force barrier. That is, the surfactant film did not form the metastable micelles that we observed on first exposure of the silica to C_{18}-TAB. This suggests that the critical process for the slow micelle to flat rearrangement occurs in the inner layer of surfactant.

Mica. Adsorption of alkyltrimethylammonium bromides on mica below the T_K is also slow to reach equilibrium. Hayes et al.[28] and Li et al.[29] have both studied the adsorption of C_{18}-TAB to mica near room temperature ($<T_K$). Hayes et al. recorded that formation of a monolayer took days when monitored ex situ, and Li et al. recorded that the monolayer formed in hours when monitored in situ. Both groups found that formation of layer proceeds via growth of islands. We also monitored adsorption of C_{18}TAB in situ at room temperature and observed the growth of islands over a period of hours. Similar behavior was observed for C_{20}TAB. However, our focus

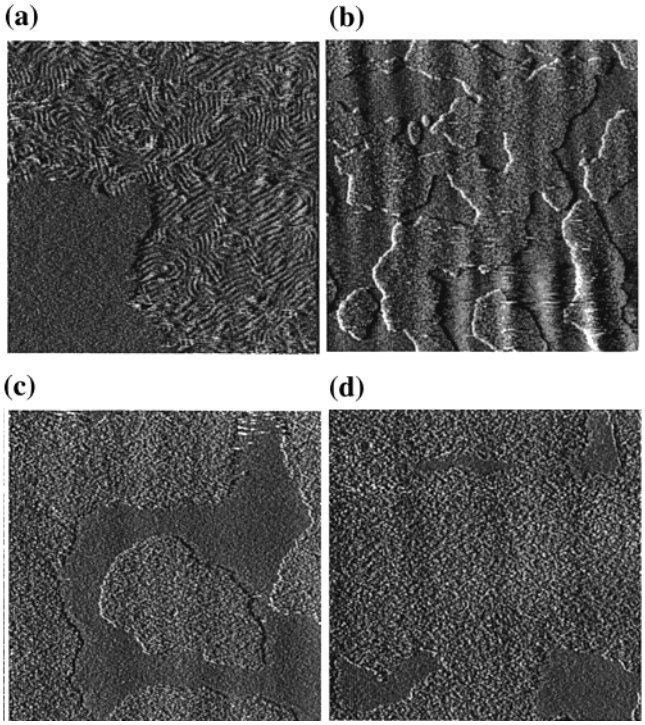

Figure 9. AFM images of structures at the interface between mica and 0.58 mM C_{18}TAB/100 mM KBr solution after the temperature was increased from 33.0 °C to 33.7 °C. None of these pictures show a steady state. (a) 0.5 μm image showing coexistence of curved cylinders and flat layers. (b) 8 μm image showing distribution of the two phases. (c) and (d): 8 μm images showing the growth of the cylinder phase over a 12 min period.

was on the organization of the adsorbate into aggregates. For C_{18}TAB and C_{20}TAB at room temperature the surfactant always formed a flat film within an island.

Above the Krafft temperature, the growth of the film was much faster and the final structure was observed minutes after injection for C_{12}TAB (cylindrical), C_{18}TAB (flat), and C_{20}TAB (flat). We have previously shown that there is a very slow (17 h) transition from a cylindrical to a flat structure for C_{16}TAB on mica.[6]

Graphite. The equilibrium structure was formed rapidly on graphite below or above T_K.

In-situ observation of Structural Transformation. Usually, transitions from one structure to another were difficult to observe. For example, when C_{18}TAB or C_{20}TAB transformed from spherical micelles to a flat sheet on silica above the Krafft temperature, the transition occurred over many hours and was observed as a gradual loss of contrast of the spheres until eventually no features were observed. In some cases, we captured very poor pictures of wormlike cylinders during the transition.

On mica, particularly in the presence of salt, the transition was easier to observe. Preliminary experiments suggest that wormlike micelles and flat sheets coexist in a stable state. (The addition of salt, an extra component, gives an extra degree of freedom compared to the surfactant-only experiments.)

Figure 9a shows wormlike cylinders and a flat layer coexisting for C_{18}TAB adsorbed to mica in 100 mM salt. Figure 9b shows a larger area under the same conditions. Although the worms are not visible on this scale, the boundary between structures can be distinguished because a constant force trace above the flat layer is 0.5 ± 0.1 nm closer to the mica. This implies that the flat sheet is thinner than the worms. Similar results were obtained for 0.58 mM C_{18}TAB and 10 mM KBr; 0.10 mM C_{20}TAB and 100 mM KBr; and 1.8 mM C_{16}TAB without KBr.

Figures 9c and 9d show the growth of the cylindrical phase resulting from an increase in temperature. When the temperature was decreased, there was an increase in the fraction of the surface covered by the flat layer.

Conclusions

Solid substrates can have a very strong influence on adsorbed surfactant organization. In contrast to bulk solution, there is not always a change in surface aggregate structure at the (bulk) Krafft temperature. Mica, silica, and graphite all exert forces strong enough to displace morphological changes at the Krafft temperature by at least 20 °C, or perhaps prevent them altogether.

Mica promotes the formation of a structure with the same symmetry as the bulk crystal, whereas graphite promotes a structure different from the bulk crystal. The effect of silica depends on the surfactant.

The ability of mica to promote the formation of a structure with the same symmetry as the surfactant crystal can be weakened by addition of KBr to solution.

On mica in KBr solution, an increase in surfactant chain length causes the same structural change as a decrease in temperature.

The bulk Krafft temperature marks a boundary in adsorption mechanism. Below T_K, adsorption proceeds via growth of islands through monomer adsorption on mica and by growth of an amorphous flat film on silica. Above T_K, adsorption is initially in the form of spherical aggregates on silica and cylindrical micelles for C_{16}TAB on mica. The change in mechanism can occur somewhat below T_K because the solid concentrates the surfactant leading to micelle formation below the cmc.

Aggregation of surfactant molecules at interfaces can occur below the (bulk) Krafft temperature. This aggregation proceeds against the electrical potential produced by the charged surfactant.

Acknowledgment. We thank Vivek Subramanian for obtaining Figure 2a, Tim Davey for providing the purified C_{20}TAB, and Mark Rutland for useful discussions. This work was supported by the National Science Foundation under contract DMR-9120004.

References and Notes

(1) Binnig, G.; Quate, C.; Gerber, G. *Phys. Rev. Lett.* **1986**, *56*, 930−933.
(2) Manne, S.; Cleveland, J. P.; Gaub, H. E.; Stucky, G. D.; Hansma, P. K. *Langmuir* **1994**, *10*, 4409−4413.
(3) Laughlin, R. G. *The Aqueous Phase Behavior of Surfactants*; Academic Press: San Diego, 1994.
(4) Israelachvili, J. N.; Mitchell, D. J.; Ninham, B. W. *J. Chem. Soc., Faraday Trans.* **1976**, *72*, 1525−1568.
(5) Wanless, E. J.; Ducker, W. A. *J. Phys. Chem.* **1996**, *100*, 3207−3214.
(6) Lamont, R. E.; Ducker, W. A. *J. Am. Chem. Soc.* **1998**, *120*, 7062−7067.
(7) Subramanian, V.; Ducker, W. A., submitted to *Langmuir*.
(8) Somasundaran, P.; Turro, N. J.; Chandar, P. *Colloids Surf.* **1986**, *20* 145−150.
(9) Campanelli, A. R.; Scaramuzza, L. *Acta Crystallogr.* **1986**, *C42*, 1380−1383.
(10) Cevc, G.; Marsh, D. *Phospholipid Bilayers*; Wiley: New York, 1987; pp 13−15.
(11) Manne, S.; Gaub, H. E. *Science* **1995**, *270*, 1480−1482.
(12) Ducker, W. A.; Grant, L. M. *J. Phys. Chem.* **1996**, *100*, 11507−11511.
(13) Manne, S.; Schäffer, T. E.; Huo, Q.; Hansma, P. K.; Morse, D. E.; Stucky, G. D.; Aksay, I. A. *Langmuir* **1997**, *13*, 6382−6387.

(14) Cyr, D. M.; Venkataraman, B.; Flynn, G. W. *Chem. Mater*. **1996**, *8*, 1600−1615.
(15) Grant, L. M.; Tiberg, F.; Ducker, W. A. *J. Phys. Chem.* **1998**, *102*, 4288−4294.
(16) Pashley, R. M.; Kitchener, J. A. *J. Colloid Interface Sci*. **1979**, *71*, 491−500.
(17) Patrick, H. N.; Warr, G. G.; Manne, S.; Aksay, I. A. *Langmuir* **1997**, *13*, 4349−4356.
(18) Ducker, W. A.; Clarke, D. R. *Colloids Surf. A* **1994**, *94*, 275−292.
(19) Fragneto, G.; Thomas, R. K.; Rennie, A. R.; Penfold, J. *Langmuir* **1996**, *12*, 6036−6043.
(20) Ducker, W. A.; Wanless, E. J. *Langmuir* **1996**, *12*, 5915−5920.
(21) Berr, S.; Jones, R. R. M.; Johnson, J. S. *J. Phys. Chem.* **1992**, *96*, 5611−5614.
(22) Swanson-Vethamuthu, M.; Feitosa, E.; Brown, W. *Langmuir* **1998**, *14*, 1590−1596.
(23) Patrick, H. N.; Warr, G. G.; Manne, S.; Aksay, I. A. *Langmuir* **1999**, *15*, 1685−1692.
(24) Isrealachvili, J. N.; Marcelja, S.; Horn, R. G. *Q. Rev. Biophys.* **1980**, *13*, 121−200.
(25) Wanless, E. J.; Ducker, W. A. *Langmuir* **1999**, *15*, 160−168.
(26) Wängerud, P.; Jönsson, B. *Langmuir* **1994**, *10*, 3542−3549.
(27) Chen, Y.-L.; Chen, S.; Frank, C.; Israelachvili, J. *J. Colloid Interface Sci*. **1992**, *153*, 244−265.
(28) Hayes, W. A.; Schwartz, D. K. *Langmuir* **1998**, *14*, 5913−5917.
(29) Li, B.; Fuji, M.; Fukada, K.; Kato, T.; Seimiya, T. *Thin Solid Films* **1998**, *312*, 20−23.